PIER C

(Received 23 December 2025, Accepted 16 March 2026, Scheduled 22 May 2026)

Comparative Analysis of Plasmonic Nanostrip Patch Antenna on Direct and Indirect Band Gap Semiconductor Substrates for Optical Applications

Poonam Namdeo, Pritam Bag, Mridula Gupta, and Biswajeet Mukherjee*

Department of Electronic Science, University of Delhi, South Campus, India

ABSTRACT: The plasmonic nanoantennas operating in the optical frequency range often experience reduced radiation efficiency due to substrate-induced nonradiative losses and insufficient electromagnetic field confinement. This work aims to systematically examine the influence of substrate material properties on plasmonic resonance behavior, surface current distribution, and radiation efficiency of a gold nanostrip patch antenna. A fixed-geometry plasmonic nanoantenna is designed and numerically investigated on five substrates, namely SiO_2, GaN, GaAs, AlAs, and AlGaAs. Full-wave electromagnetic simulations are performed using frequency-dependent material dispersion modelled through established Drude-Lorentz formulations. The antenna implemented on the Au-SiO_2 combination provides the most favourable plasmonic performance, yielding the best impedance matching (-51.27 dB), maximum radiation efficiency of 83%, wide impedance bandwidth (118 THz), and highly stable radiation patterns. GaN also exhibits strong performance with a high radiation efficiency (71%) and wide bandwidth (97 THz), making it a viable choice for high-power optical systems. GaAs, AlAs, and AlGaAs substrates show reduced efficiency due to higher dielectric losses and weaker plasmonic confinement. The study confirms that substrate permittivity and loss characteristics play a crucial role in determining plasmonic nanoantenna performance.

1. INTRODUCTION

The rapid evolution of optical communication technologies has created a growing demand for compact, efficient, and highly integrated radiating elements capable of operating beyond the microwave spectrum [1, 2]. Among these, plasmonic nanoantennas have emerged as promising candidates owing to their ability to confine and manipulate electromagnetic energy at dimensions far below the diffraction limit [3, 4]. By exploiting surface plasmon polaritons (SPPs) generated at metal-dielectric interfaces, nanoantennas enable strong field localization, enhanced light matter interaction and improved radiation control at optical frequencies [5, 6]. Unlike conventional microwave antennas, the electromagnetic behavior of nanoantennas is strongly governed by the dispersive nature of metals and the dielectric properties of the surrounding medium [7, 8]. At optical frequencies, metals no longer behave as perfect conductors; instead their response is accurately described using the Drude dispersion model, which accounts for the collective oscillation of free electrons [9]. Consequently, both the metallic layer and the dielectric substrate play a crucial role in determining resonance characteristics, radiation efficiency, impedance matching, and overall antenna performance [10, 11]. Among various nanoantenna geometries, plasmonic nanostrip, and patch-based structures have attracted considerable attention due to their compact geometry, fabrication feasibility, and strong resonant behavior [4]. These structures support multiple transverse magnetic (TM) modes, enabling effective control over resonance frequency, field distribution and radiation characteristics [12, 13]. However, the efficiency and bandwidth of these modes are highly sensitive to the dielectric environment surrounding the antenna. In recent years, several dielectric and semiconductor substrates, such as Silicon Dioxide (SiO_2), Gallium Arsenide (GaAs), Gallium Nitride (GaN), Aluminum Arsenide (AlAs), and Aluminum Gallium Arsenide (AlGaAs) have been explored for plasmonic and optical applications [14–16]. Each of these materials exhibits distinct electromagnetic properties, including relative permittivity, loss tangent, and band-gap energy, which significantly influence the propagation and radiation behavior of surface plasmons. Despite extensive studies, a systematic comparison of these substrate materials under identical antenna configurations remains limited [17]. Motivated by this research gap, the proposed work introduces a substrate-antenna co-optimization framework that reveals the physical balance between radiative and nonradiative decay mechanisms, enabling efficient plasmonic nanoantenna operation without increasing structural complexity. The proposed work investigates a plasmonic nanostrip patch antenna operating in the optical frequency range using gold as the plasmonic conductor [18]. A comparative performance analysis is carried out for different dielectric substrates to evaluate key antenna parameters such as resonant frequency, reflection coefficient, radiation efficiency, gain, and radiation pattern. The metal is modelled using the Drude dispersion model, while frequency-dependent dielectric properties are incorporated to ensure accurate electromagnetic characterization [19, 20]. The objective of this study is to iden-

* Corresponding author: Biswajeet Mukherjee (biswajeet.26@gmail.com).

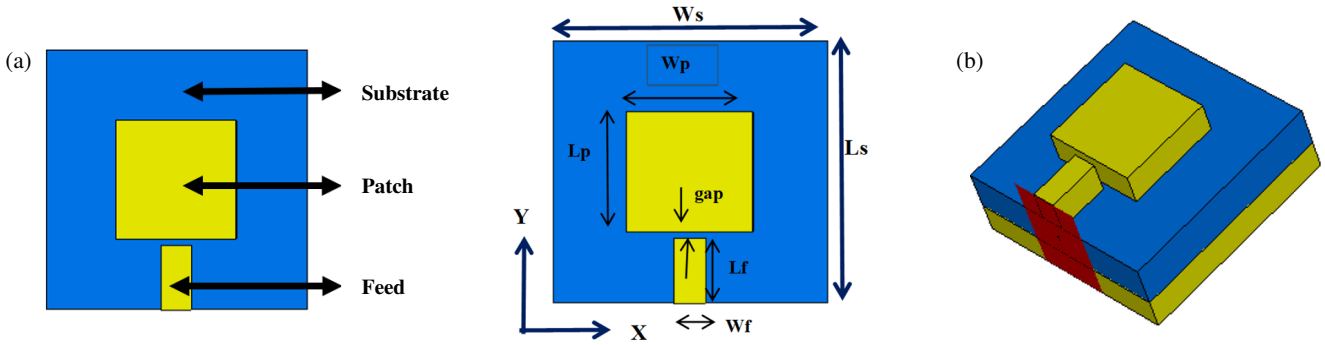

FIGURE 1. Configuration of proposed antenna. (a) Top view. (b) Perspective view.

TABLE 1. Geometrical parameters and material properties of the proposed nanoantenna.

Semiconductor Substrates	Parameter Values (nm)							
	Length of Patch (L_p)	Width of Patch (W_p)	Width of Feed line (W_f)	Length of Substrate (L_s)	Width of Substrate (W_s)	Height of patch (H_g)	Height of Substrate (H_s)	Gap
SiO_2 (Indirect band gap)	480	480	120	1050	1050	150	200	25
GaN (Direct band gap)	480	480	120	1080	1080	180	180	25
GaAs (Direct band gap)	480	480	120	1050	1050	150	150	25
AlAs (Direct band gap)	480	480	120	1080	1080	130	122	25
AlGaAs (Direct band gap)	480	480	120	1080	1080	120	120	25

tify the most suitable metal-substrate combination for high-performance optical frequency plasmonic operation and to provide insights into material-dependent performance variations for next-generation optical communication [4, 21].

2. GEOMETRY OF PLASMONIC NANO-STRIP PATCH ANTENNA

2.1. Configuration and Design Methodology

Figures 1(a) and (b) show the geometry and dimensional configuration of the proposed plasmonic nanostrip patch antenna, where W_s, L_s, and H_s are the width, length, and height of the substrate; W_p, L_p, and H_g are the width, length and height of the patch, respectively; W_f is the width of the feed line, and gap-coupled feed was introduced to enhance impedance matching.

The antenna consists of a square gold (Au) patch placed on a dielectric substrate with gold thickness maintained at the nanoscale to support efficient plasmonic excitation [4]. Five substrates were evaluated: SiO_2, GaN, GaAs, AlAs, and AlGaAs, which were selected owing to their varying dielectric constants, bandgap classifications, and optical loss characteristics.

The width and length of a nanostrip patch antenna are typically selected to correspond to the plasmonic mode resonance condition. The effective wavelength and the antenna length are typically correlated.

The length of the antenna is related to the effective wavelength λ_{eff} of the metal, which is given by [4, 21] the following equation:

$$\lambda_{eff} \approx \frac{\lambda}{\sqrt{\varepsilon_r(\omega)}} \tag{1}$$

where λ is the free space wavelength at the resonant frequency, $\varepsilon_r(\omega)$ is the relative dielectric constant of the metal at the resonant frequency, thus, the length of the patch can be approximated by [4, 21] the following equation:

$$L_p \approx \frac{\lambda}{2\sqrt{\varepsilon_r(\omega)}} \tag{2}$$

The same formula can also be used to obtain the width W_p of the nanostrip patch antenna. The width of the feed line was determined via impedance matching at the operating frequency. The detailed geometrical dimensions and material parameters of the proposed nano antenna are listed in Table 1. Computer Simulation Technology (CST) Microwave Studio was used to perform the parametric analysis [22, 23].

TABLE 2. Drude and Lorentz model values for different substrate materials.

Material	Model	ε_s	ε_∞	ω_p (rad/s)	ω_r (rad/s)	ω_c (rad/s)
Gold (Au)	Drude	-	9.5	1.37×10^{16}	-	4.05×10^{13}
SiO_2	Lorentz	3.9	2.1	-	1.0×10^{14}	1.0×10^{12}
GaN	Lorentz	9.5	5.35	-	8.0×10^{13}	1.2×10^{13}
GaAs	Lorentz	12.9	10.9	-	7.5×10^{13}	1.5×10^{13}
AlAs	Lorentz	10.8	8.2	-	7.0×10^{13}	1.4×10^{13}
AlGaAs	Lorentz	9.8	9.8	-	7.2×10^{13}	1.6×10^{13}

2.2. Understanding the Structural Configuration and Metal Dielectric Function

Knowing the dielectric function of the metal at the intended frequency is essential for developing plasmonic antennas at optical wavelengths. Plasmonic resonance can be ascertained using the frequency-dependent dielectric function $\varepsilon(\omega)$ of a metal, which is calculated using the Drude dispersive model at optical frequency since only intra-band transitions are significant in conductors. The semiconductor and insulators were modelled using the Lorenz model, which includes both intra-band and inter-band transitions [21, 24]. The model Equations are stated in (3) and (4).

Drude mode [21, 24, 25]

$$\varepsilon(\omega) = \varepsilon_\infty - \frac{\omega p^2}{\omega(\omega + j\omega c)} \tag{3}$$

Lorenz Model [21, 24, 25]

$$\varepsilon(\omega) = \varepsilon_\infty + \frac{(\varepsilon_s - \varepsilon_\infty)\omega r^2}{\omega r^2 + j\omega\delta - \omega^2} \tag{4}$$

where ω_p = plasma frequency, ω_c = collision frequency of the incident wave, ω_r = the resonant frequency, δ = the damping factor, ε_s = the static permittivity and ε_∞ = the permittivity at $\omega = \infty$.

The extracted resonant frequencies for the metals and substrates based on the Drude and Lorentz dispersion models are shown in Table 2.

2.3. Material Modelling and Electromagnetic Properties

In the present work, the metallic component of the nanoantenna is modelled using the classical Drude dispersion model [21], which effectively describes the frequency-dependent response of free electrons in noble metals. This model captures the collective oscillation of conduction electrons and accounts for intrinsic material losses through a collision frequency parameter. The frequency-dependent complex permittivity of the metal [24] is expressed as a function of plasma frequency and damping constant, allowing realistic simulation of plasmonic resonance phenomena.

Gold (Au) is selected as the plasmonic material due to its chemical stability, low oxidation tendency, and well-established plasmonic performance in the optical range. The dispersive behaviour of gold enables the strong confinement of electromagnetic fields at the metal-dielectric interface, leading to enhanced surface plasmon polariton excitation [25, 26]. The accurate representation of this dispersive response is essential for predicting resonance shifts, field enhancement, and radiation efficiency.

2.4. Selection of Substrates for Designing of Nanoantenna

The choice of the correct dielectric material depends on a number of different features, such as the resonant frequency, which is a function of the dimensions, shape, and Q factor of the material [26].

The dielectric material SiO_2 is generally used for nanoantenna in high-frequency applications because it exhibits low dielectric and hysteresis losses, low polarization, high thermal stability, high purity, and chemical stability. GaN dielectric materials offer a range of benefits for high- frequency applications, including high-power handling, excellent temperature management, fast electron mobility, and high efficiency at high frequencies. The GaAs dielectric offers several key advantages, such as low-noise characteristics, high-power handling, and high breakdown voltage. The AlAs dielectric plays a crucial role in improving the performance of high-frequency application, contributing to better power handling, efficient carrier confinement, and stable operation. The AlGaAs dielectric material offers advantages in the high-frequency region owing to its wideband-gap, low noise characteristics, and improved power efficiency, which makes it suitable for use in optical communication systems [27].

The SiO_2 has a high positive real permittivity and refractive index in the optical frequency region and a lower extinction coefficient [21], which is most suitable for high-frequency performance compared to the other substrates.

2.5. Optimization of Gap Coupled Feed

For effective energy coupling, the gap distance between the radiating patch and the feed was optimized. Usually, this gap is extremely small, of the order of nanometres. By optimizing the coupling coefficient k between the feed and patch, a gap can be found which is explained by [4]:

$$K \approx \frac{Z_0}{Z_0 + j\frac{\omega C}{d}} \tag{5}$$

where Z_0 is the feed impedance, C is the capacitance between the feed and patch, and d is the gap.

3. RESULT AND ANALYSIS

The performance of the proposed plasmonic nanoantenna is evaluated through comprehensive electromagnetic simulations to investigate its resonant behavior, radiation characteristics, and material-dependent response. The results presented in this section highlight the influence of substrate material properties on the antenna's operational characteristics, including reflection coefficient, resonant frequency, field distribution, and radiation efficiency.

3.1. Analysis of the Reflection Coefficient Using Substrates

A lower $|S_{11}|$ value indicates better impedance matching and higher coupling efficiency between the feed and plasmonic radiating element. Fig. 2 shows the combined $|S_{11}|$ characteristics of the proposed plasmonic nanostrip patch antenna (NPA) on five different substrate materials namely SiO_2, GaN, GaAs, AlAs, and AlGaAs. Each substrate exhibited two distinct resonant frequencies, corresponding to higher-order plasmonic modes supported by the square nanostrip geometry at optical frequencies.

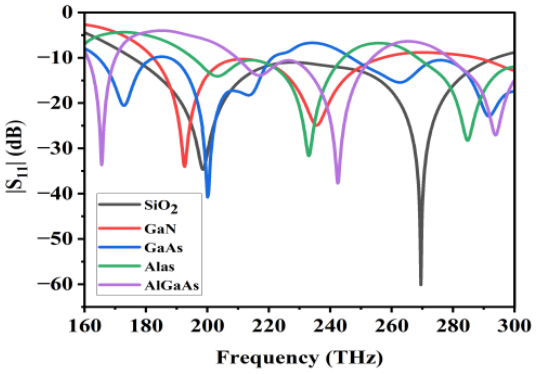

FIGURE 2. Simulated reflection coefficient $|S_{11}|$ of the proposed nanoantenna for different substrate materials.

On the SiO_2, the antenna exhibits resonant frequencies at 198.41 THz and 269.62 THz with corresponding reflection coefficients of −35.14 dB and −51.67 dB respectively. The extremely low $|S_{11}|$ value (269.62 THz) indicates exceptionally strong plasmonic coupling between the gold patch and the SiO_2 substrate. This is due to the low dielectric constant ($\varepsilon_r \approx 3.7$–$3.9$), minimal dielectric loss tangent, and strong surface plasmon polarization (SPP) support at the Au-SiO_2 interface. These properties allow efficient energy transfer, producing the deepest and cleanest resonance dips among all substrates.

For GaN, the antenna resonated frequencies at 182 THz and 237 THz with corresponding reflection coefficients of −34 dB and −25 dB. Although the resonances are not as deep as those for SiO_2, GaN still performs well because of its high electron mobility, wide bandgap energy (3.4 eV), and moderate permittivity ($\varepsilon_r \approx 8.9$–$10.6$). These properties facilitate a stable plasmonic behavior and moderate field confinement. Therefore, GaN serves as a strong candidate for high-power and high-temperature optical applications.

On GaAs, the antenna resonated at frequencies 173 THz and 200 THz with corresponding reflection coefficients of −21 dB and −37 dB. Although it achieves a good second dip at −37 dB, the first resonance is relatively weak (−21 dB), indicating imperfect coupling at that frequency. This leads to a moderate reflection coefficient performance compared with that of SiO_2 and GaN.

For AlAs, antenna resonances were observed at 209 THz and 244 THz, achieving reflection coefficient of −15 dB and −31.67 dB, respectively. The first resonance dip was shallow, suggesting insufficient coupling and a significant reflection at the feed. Thus, the performance of AlAs was below SiO_2, GaN, and GaAs.

Similarly, on an AlGaAs substrate, the antenna resonates at 205 THz and 235 THz, characterized by reflection coefficients of −14 dB and −39 dB, respectively. The second resonance is sharp (−39 dB), and the first is extremely poor (−14 dB), indicating a strong mismatch at lower THz frequencies. Because AlGaAs is a composite alloy, it exhibits greater optical dispersion, increased carrier scattering, and higher losses than other substrates. These factors degrade the reflection characteristics, making AlGaAs a weaker-performing substrate.

From the reflection coefficient analysis, it is evident that SiO_2 produces the most efficient resonance behavior with the sharpest and deepest reflection minima. GaN also displays good impedance characteristics and is suitable for practical optical applications. The remaining substrates, show inferior impedance matching and higher reflection, resulting in weaker nanoantenna performance.

3.2. Analysis of the Radiation Efficiency Using Substrates

Radiation efficiency is a critical performance indicator for plasmonic nanoantennas, as it quantifies how effectively the antenna converts the accepted input power into radiated electromagnetic energy. At optical frequencies, radiation efficiency is strongly influenced by the dielectric constant, optical loss, and plasmonic compatibility between the metal and substrate. Thus, the choice of the substrate material plays a central role in determining the overall antenna performance.

Figure 3 shows the radiation efficiency using five substrates (SiO_2, GaN, GaAs, Alas, and AlGaAs) of the designed Square-shaped Nano-antenna. The SiO_2 Nano structure showed a radiation efficiency of 83 percent at 198.41 THz and 78 percent at 269.62 THz frequency. This excellent performance results

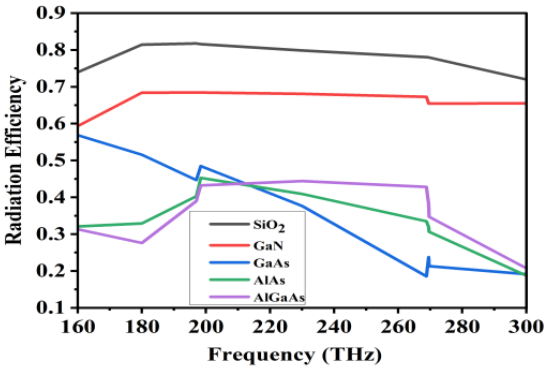

FIGURE 3. Radiation efficiency of the proposed nanoantenna for different substrate materials.

TABLE 3. Variation of NPA parameters with different substrate materials.

PA with different type substrate materials	Resonant frequency @THz	Gain (dB)	Directivity	Radiation Efficiency (%)	HPBW (deg.)	S_{11} (dB)	Maximum-radiation Efficiency (%) @THz	Bandwidth (F_U-F_L) (@THz)	Bandwidth (%)
SiO_2	Fr1 = 198.41	5.39	6.27	82	153.80	−35.14	83	175–293 (118)	50.42
	Fr2 = 269.62	7.7	7.12	78	93	−51.67			
GaN	Fr1 = 182	3.98	5.63	69	98.90	−34	71	168–265 (97)	44.80
	Fr2 = 237	4.32	625	65	86	−25			
GaAs	Fr1 = 173	3.71	6.56	52	104.80	−21	55	163–220 (57)	29.76
	Fr2 = 200	2.2	5.35	49	77	−37			
AlAs	Fr1 = 209	4.54	7.99	47	87.40	−15	48	200–257 (57)	29.76
	Fr2 = 244	2.8	7.76	33	48.90	−31.67			
AlGaAs	Fr1 = 205	4.18	7.71	45	86.50	−14	47	196–247 (51)	23.02
	Fr2 = 235	2.24	6.86	35	49	−39			

from a low dielectric constant ($\varepsilon_r \approx 3.7$–$3.9$), which minimizes dielectric energy trapping. These properties allow more guided plasmonic mode energy to be released into free space, producing superior radiation efficiency compared to all other substrates.

GaN shows a radiation efficiency of 69 percent at 182 THz and 65 at 237 THz. Moderately high permittivity of GaN ($\varepsilon_r \approx 8.9$–$10.6$) introduces additional dielectric loading but maintains a reasonably strong field confinement. Thus, GaN delivers stable and high radiation efficiency, making it a solid candidate for optical communication systems [23, 24].

GaAs exhibits a radiation efficiency of 55 percent at 173 THz and 50 at a frequency of 200 THz. The reduction in efficiency is primarily caused by GaAs's higher dielectric constant ($\varepsilon_r \approx 10.9$–$12.9$), which increases the energy storage inside the substrate and internal power losses. As a result, less power is radiated into free space, and overall efficiency decreases with that of SiO_2 and GaN.

AlAs show radiation efficiencies of 48 percent at 209 THz and 33 percent at 244 THz. AlAs suffer from higher damping at optical frequencies. The reduced efficiency reflects significant substrate-induced energy dissipation.

AlGaAs shows a radiation efficiency of 46 percent at 205 THz and 35 percent at 235 THz. As a composite alloy with varying Al/Ga ratios, AlGaAs introduces higher optical dispersion. These mechanisms significantly weaken the plasmonic fields on the gold surface, causing substantial power loss before it reaches the radiation.

The radiation efficiency analysis confirmed that SiO_2 is the most effective substrate for plasmonic nanoantenna operation in the optical region, providing the highest efficiency and minimal losses. GaN also offers strong performance, and GaAs, AlAs, and AlGaAs exhibit degraded efficiency.

3.3. Analysis of the Normalized Radiation Pattern on the Substrates

Figure 4 shows the normalized radiation pattern for substrate materials SiO_2 and GaN, at their respective resonant frequencies for the designed plasmonic square-shaped nano patch antenna. The radiation patterns were evaluated in terms of the co-polarized and cross-polarized field components to determine the quality of radiation, polarization purity, and overall stability of the antenna performance in the optical region.

Figure 4(a) shows the normalized far-field pattern of SiO_2 substrate. The co-pol component exhibits clear broadside radiation, while the cross-pol level remains significantly lower, indicating excellent polarization purity. The SiO_2 based antenna produces a pattern close to an ideal square patch radiator in the optical range and maintains good lobbing stability across both resonant frequencies. The cross-polar components are less than 20 dB of the co-polar components, satisfying the linear polarization of the antenna.

Figure 4(b) illustrates the normalized far-field pattern of the GaN substrate, shows a slightly narrower main lobe compared to SiO_2. The high electron mobility of GaN supports improved plasmonic confinement but also introduces dielectric losses, which affect the inversed cross-polar levels. Nevertheless, GaN delivers robust performance suitable for high-power nanoscale photonic applications. The normalized far-field pattern also analysed for GaAs, AlAs, and AlGaAs substrates, which shows lower main-lobe peak, increased asymmetry, and reduced polarization purity compared to SiO_2 and GaN.

Overall, the normalized radiation patterns confirm that the substrate permittivity and optical dispersion strongly influence the far-field behavior of the plasmonic nanostrip antennas. Among all the materials, SiO_2 demonstrates the most desirable radiation characteristics for optical communication systems, including a well-defined main lobe, low sidelobe distortion, and excellent polarization purity. GaN also shows promising behavior, whereas GaAs, AlAs, and AlGaAs suffer from greater cross-polarization and pattern broadening.

3.4. Analysis of the Surface Current and Magnetic Field on the Substrates

To gain physical insight into plasmonic resonance behavior, the surface current distributions at the resonant frequencies are

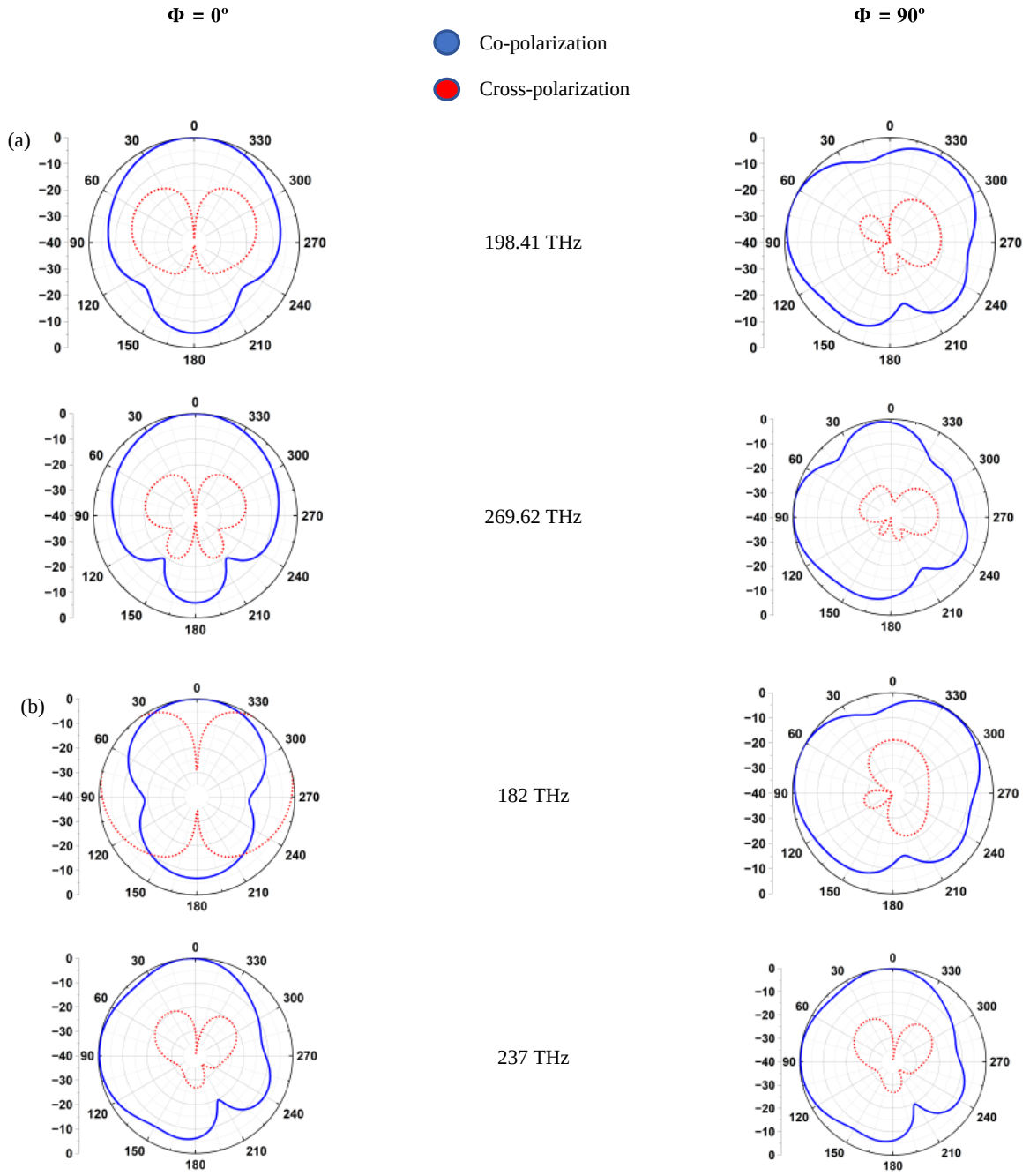

FIGURE 4. Normalized radiation patterns of the proposed nanoantenna with different substrate materials. (a) SiO_2. (b) GaN.

presented in Figs. 5–6. Figs. 5(a), (b) for the SiO_2 substrate, well-defined standing-wave surface currents at 198.41 THz and 269.62 THz exhibit strong spatial overlap with uniformly distributed H-field loops, indicating minimal dielectric loss and effective plasmonic energy confinement. This strong current-field coupling directly results in deep impedance minima and high radiation efficiency. Figs. 6(a), (b) on GaN substrate exhibit good field confinement and slightly disordered surface currents due to a stronger dielectric loading. The surface current and magnetic field also analysed for GaAs, AlAs, and AlGaAs substrates, which shows asymmetrical H-field distribution and surface currents become less concentrated compared to SiO_2 and GaN.

The entire field distribution analysis clearly demonstrates that SiO_2 provides the strongest plasmonic confinement and highest surface current density, making it the most effective substrate for THz plasmonic nanoantenna applications. GaN is the second-best, with moderate field leakage but strong performance. GaAs, AlAs, and AlGaAs progressively degrade the plasmonic resonance, causing distorted H-field behavior and fragmented surface currents.

3.5. Analysis of the Gain, Directivity, Bandwidth, and Half Power Beamwidth for the Substrates

To further understand the radiative behaviour of the proposed plasmonic nanostrip patch antenna (NPA), the gain, directiv-

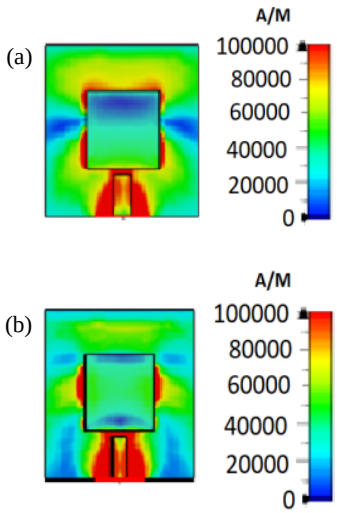

FIGURE 5. Surface current distribution of nano patch antenna with substrate SiO_2. (a) 198.41 THz, (b) 269.62 THz.

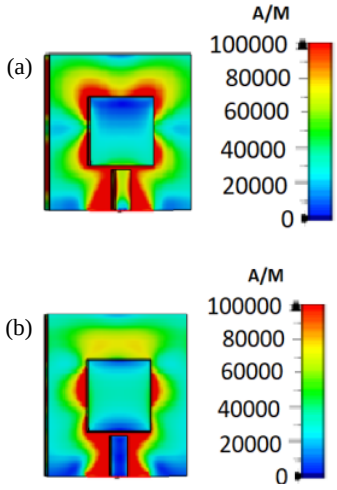

FIGURE 6. Surface current distribution of nano patch antenna with substrate GaN. (a) 182 THz, (b) 237 THz.

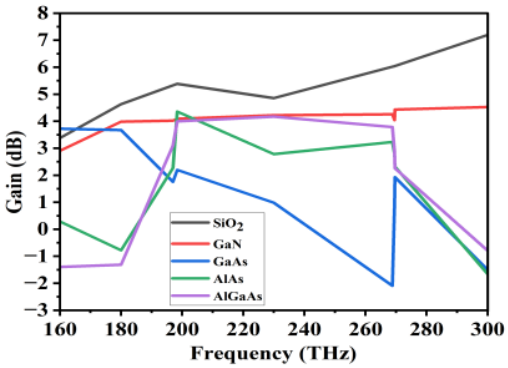

FIGURE 7. Gain analysis of the proposed nanoantenna for different substrate materials.

ity, impedance bandwidth, and half-power beamwidth (HPBW) were evaluated for each of five substrates (SiO_2, GaN, GaAs, AlAs, and AlGaAs) at their corresponding resonant frequencies. These parameters provide essential information about the antenna's capability to efficiently radiate power, maintain directional stability, and operate over a broad frequency range in the optical domain. A performance comparison based on the extracted results is summarized in Table 3.

3.5.1. Gain Analysis

Figure 7 shows that SiO_2 exhibits the highest gain among all substrates, achieving 7.7 dB at 269.62 THz and 5.39 dB at 198.41 THz. This strong performance is attributed to its low dielectric constant, minimal optical absorption, and Superior SPP confinement at the Au-SiO_2 interface. These factors enhance the radiation efficiency and reduce power dissipation within the substrate. GaN demonstrated moderate gain values of 4.32 dB at 237 THz and 3.98 dB at 182 THz. Its higher permittivity leads to greater dielectric loading but maintains reasonable plasmonic confinement owing to the high electron mobility of GaN.

GaAs, AlAs, and AlGaAs offer high-permittivity substrates that yield significantly lower gains (2–4.5 dB range). This reduction is caused by increased substrate loss, stronger field penetration into the dielectric, and weaker plasmonic resonance strength. Thus, less energy is radiated into free space, lowering the effective gain.

3.5.2. Directivity Analysis

As is evident from far field plots, SiO_2 shows the highest directivity (up to 7.12 dB) owing to the well-formed broadside radiation and low cross-polarization components, GaN shows moderate directivity ($\approx$ 5.6–6.25 dB) and GaAs, AlAs, and AlGaAs show reduced directivity ($\approx$ 5–7.9 dB) with increased beam distortion and broader radiation patterns.

3.5.3. Impedance Bandwidth Effects

SiO_2 provides a maximum impedance bandwidth of 118 THz (175–293 THz), which is significantly superior to that of all other substrates. This wideband response is associated with enhanced impedance matching, strong plasmonic resonance coupling, and low dispersion in the SiO_2 medium. GaN shows a substantial bandwidth of 97 THz, making it suitable for optical systems. For GaAs, AlAs, and AlGaAs substrates, narrower bandwidths ranging from 51–57 THz were observed due to higher optical dispersion, increased dielectric absorption, and weaker loading of surface plasmon modes.

3.5.4. Parametric Optimization

Substrate height (H_s), one of the structural parameters, plays a dominant role in determining the plasmonic resonance behavior, radiation efficiency, impedance matching, and field distribution of the antenna. To achieve optimal operation, a detailed parametric investigation of the substrate height was performed for each of the five substrates SiO_2, GaN, GaAs, AlAs, and AlGaAs. The results of this parametric study are shown in Fig. 8,

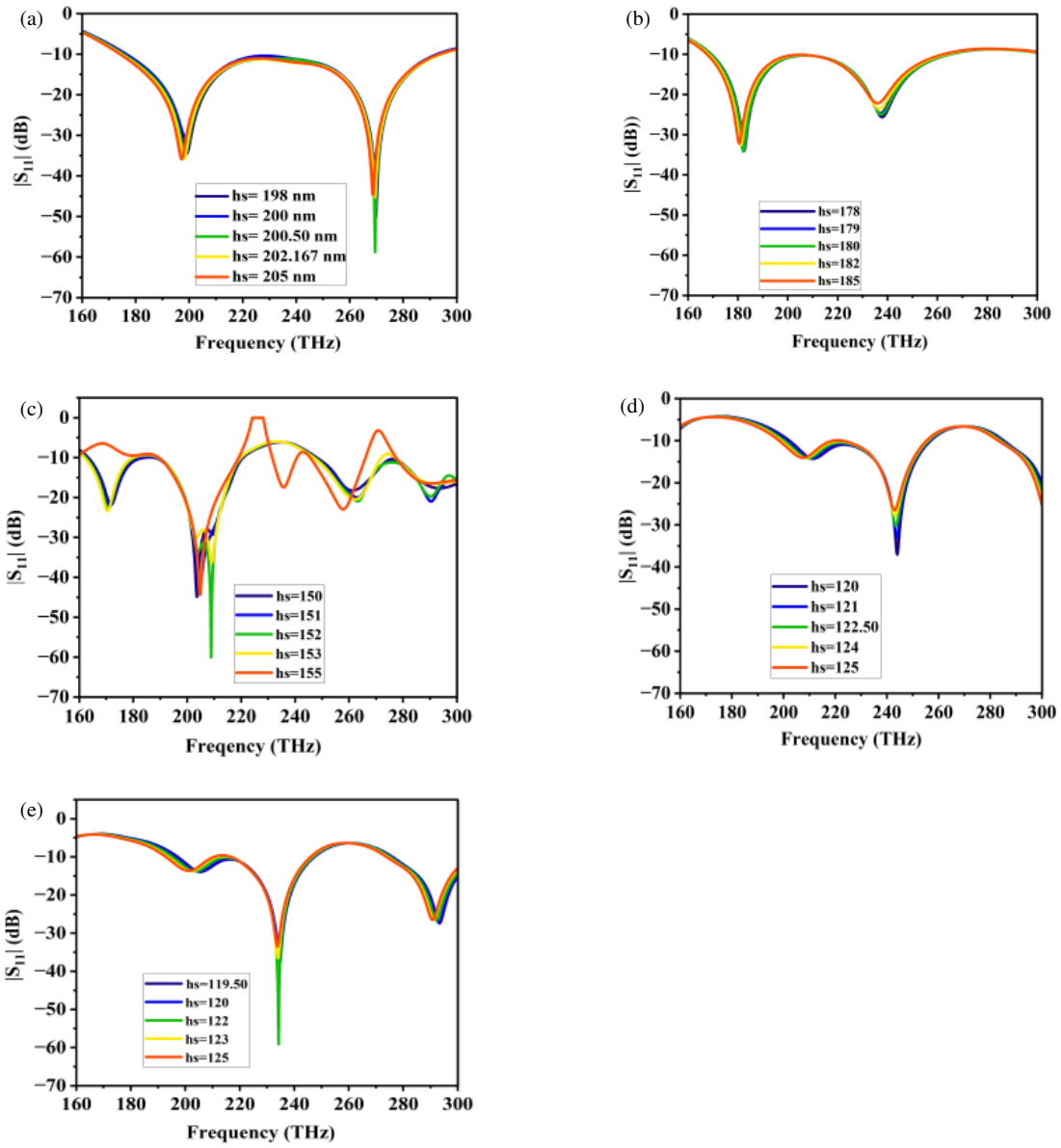

FIGURE 8. Variation of height of substrates in parameter optimization. (a) SiO_2. (b) GaN. (c) GaAs. (d) AlAs. (e) AlGaAs.

where the response of the nanostrip patch antenna to variations in substrate height is examined in terms of resonance shifting, reflection coefficient behaviour and overall stability of the plasmonic modes.

As shown in Fig. 8(a), SiO_2 showed the most stable response to the substrate-height variation. The optimal height of 200 nm provided the deepest $|S_{11}|$ resonance (-51.67 dB) strongest plasmon confinement, and maximum radiation efficiency (83%). Increasing the height beyond $\sim$220 nm results in minor resonance broadening, while reducing it below 180 nm leads to a significant impedance mismatch owing to increased field leakage into free space.

For GaN in Fig. 8(b), the optimal height is 180 nm, which yields balanced impedance matching, well-defined dual-band resonances, and a moderate radiation efficiency (69% at Fr1). A larger height (> 200 nm) increases the dielectric absorption, whereas smaller heights (< 150 nm) lead to underdeveloped plasmon modes and inefficient field confinement.

The optimal height of GaAs (Fig. 8(c)) was found to be 150 nm. At this height, dual resonances exhibit improved sharpness and radiation efficiency stabilizes at around 50–55%, and heights beyond 170 nm cause noticeable power trapping within the substrate owing to its high ε_r, while thinner substrates degrade modal stability.

As shown in Fig. 8(d), for AlAs, the optimal height is approximately 122 nm At this value, $|S_{11}|$ reaches its minimum (-31.67 dB at Fr2) and the fields remain moderately confined at the Au-AlAs boundary.

For AlGaAs, Fig. 8(e) shows the strongest sensitivity to substrate height variations owing to its composite dielectric nature. The optimal height was 120 nm, at which resonance dips became more pronounced and field confinement improved com-

pared to other height values. Beyond 130 nm, the absorption and scattering losses become significant, adversely affecting antenna performance.

The parameter optimization study clearly demonstrated that the substrate height must be tailored individually for each dielectric material to ensure optimal plasmonic resonance and radiation behavior. The proposed substrate-antenna co-optimization approach provides practical design guidelines for the development of efficient plasmonic nanoantennas in optical communication, sensing, and nanoscale photonic systems [28–30].

4. CONCLUSION

This study presents the design and comparative investigation of a plasmonic nanostrip patch antenna operating in the optical frequency range using gold (Au) as the plasmonic conductor. The antenna performance was systematically evaluated on five semiconductor substrates, namely SiO_2, GaN, GaAs, AlAs, and AlGaAs, while maintaining identical antenna geometry. To accurately capture the electromagnetic behavior at optical frequencies, the metal was modeled using the Drude dispersion model and the dielectric substrates were characterized using the Lorentz model. Full-wave simulations were carried out to analyze key performance parameters including reflection coefficient, radiation efficiency, gain, bandwidth, and radiation patterns. The obtained results clearly demonstrate that the dielectric substrate plays a critical role in determining plasmonic resonance behavior and radiation performance. Among the investigated materials, the Au-SiO_2 configuration exhibits the most favorable characteristics, achieving the maximum reflection coefficient of -51.67 dB, maximum radiation efficiency of 83%, and a wide impedance bandwidth of 118 THz. The SiO_2 substrate also provides stable radiation patterns with low cross-polarization levels, indicating strong surface plasmon confinement and efficient electromagnetic radiation. The Au-GaN combination also demonstrates promising performance with radiation efficiency up to 71% and a bandwidth of 97 THz, making it a suitable alternative for high-frequency optical applications. In contrast, substrates with higher dielectric permittivity and optical losses such as GaAs, AlAs, and AlGaAs exhibit weaker plasmonic confinement, resulting in reduced radiation efficiency and a narrower bandwidth. The novelty of this work lies in the systematic substrate-dependent performance comparison under identical antenna configurations, providing clear physical insight into the relationship between substrate permittivity, plasmonic confinement, and radiation efficiency.

ACKNOWLEDGEMENT

The authors acknowledge the support of the DU Institute of eminence and project TTDF/6G/111.

REFERENCES

[1] Boltasseva, A. and H. A. Atwater, "Low-loss plasmonic metamaterials," *Science*, Vol. 331, No. 6015, 290–291, 2011.

[2] Maier, S. A., M. L. Brongersma, P. G. Kik, S. Meltzer, A. A. G. Requicha, and H. A. Atwater, "Plasmonics — A route to nanoscale optical devices," *Advanced Materials*, Vol. 13, No. 19, 1501–1505, 2001.

[3] Bharadwaj, P., B. Deutsch, and L. Novotny, "Optical antennas," *Advances in Optics and Photonics*, Vol. 1, No. 3, 438–483, 2009.

[4] Kashyap, N., Z. A. Wani, R. Jain, Khusboo, and V. D. Kumar, "Investigation of a nanostrip patch antenna in optical frequencies," *Applied Physics A*, Vol. 117, No. 2, 725–729, 2014.

[5] Vasa, P. and C. Lienau, "Strong light-matter interaction in quantum emitter/metal hybrid nanostructures," *ACS Photonics*, Vol. 5, No. 1, 2–23, 2018.

[6] Kaniber, M., K. Schraml, A. Regler, J. Bartl, G. Glashagen, F. Flassig, J. Wierzbowski, and J. J. Finley, "Surface plasmon resonance spectroscopy of single bowtie nano-antennas using a differential reflectivity method," *Scientific Reports*, Vol. 6, No. 1, 23203, 2016.

[7] Ahmad, W., Y. Wang, G. Du, Q. Yang, and F. Chen, "Graphene-based plasmonic antenna for advancing nano-scale sensors," *Nanomaterials*, Vol. 15, No. 12, 943, 2025.

[8] Butt, M. A., "Plasmonics meets metasurfaces: A vision for next generation planar optical systems," *Micromachines*, Vol. 17, No. 1, 119, 2026.

[9] Coviello, V., D. Badocco, P. Pastore, M. Fracchia, P. Ghigna, A. Martucci, D. Forrer, and V. Amendola, "Accurate prediction of the optical properties of nanoalloys with both plasmonic and magnetic elements," *Nature Communications*, Vol. 15, No. 1, 834, 2024.

[10] Moazen Dehkordi, S. and H. Mohammadi, "Improvement of directivity in plasmonic nanoantennas based on structured cubic gold nanoparticles," *Scientific Reports*, Vol. 14, No. 1, 17153, 2024.

[11] Sekrafi, H. E., D. S. Costa, M. Proença, D. I. Meira, F. Vaz, and J. Borges, "Experimental and theoretical studies on Ag nanoparticles with enhanced plasmonic response, formed within Al_2O_3 thin films deposited by magnetron sputtering," *Plasmonics*, Vol. 19, No. 6, 3177–3188, 2024.

[12] Coello, V., M. A. Abdulkareem, C. E. Garcia-Ortiz, C. T. Sosa-Sánchez, R. Téllez-Limón, and M. Peña-Gomar, "Plasmonic coupled modes in a metal-dielectric periodic nanostructure," *Micromachines*, Vol. 14, No. 9, 1713, 2023.

[13] Dmitriev, P. A., E. Lassalle, L. Ding, Z. Pan, D. C. J. Neo, V. Valuckas, R. Paniagua-Dominguez, J. K. W. Yang, H. V. Demir, and A. I. Kuznetsov, "Hybrid dielectric-plasmonic nanoantenna with multiresonances for subwavelength photon sources," *ACS Photonics*, Vol. 10, No. 3, 582–594, 2023.

[14] Faramarzi, V., S. Vatani, M. Heidari, J. Park, and M. T. Hwang, "Plasmonic resonance modulation of graphene by nanoscale substrate curvatures," *Nanoscale Advances*, Vol. 7, No. 24, 7899–7912, 2025.

[15] Alsayed, A. E., A. M. Ghanim, A. Yahia, and M. A. Swillam, "Giant localized electromagnetic field of highly doped silicon plasmonic nanoantennas," *Scientific Reports*, Vol. 13, No. 1, 5793, 2023.

[16] Zhu, H., Y. Chu, F. Shang, L. Zhang, Y. Chen, H. Wang, Z. Chen, Q. Hou, L. Chen, W. Qin, Z. Cheng, and Y. Zhang, "Plasmon-enhanced absorption in dielectric layer coated III-V nanowire array decorated with nanoparticles," *Optical Materials*, Vol. 162, 116922, 2025.

[17] Esfahani, N. E., J. Kovác Jr., G. Maruccio, S. Rizzato, and S. Kovácová, "Comparative analysis of two different mim configurations of a plasmonic nanoantenna," *Plasmonics*, Vol. 20, No. 6, 3265–3279, 2025.

[18] Raeen, M. S., A. Nella, and R. W. Aldhaheri, "A high-performance ultra-compact plasmonic metamaterial structure for

optical THz absorption," *Scientific Reports*, Vol. 14, No. 1, 27203, 2024.

[19] Indhu, A. R., L. Keerthana, and G. Dharmalingam, "Plasmonic nanotechnology for photothermal applications — An evaluation," *Beilstein Journal of Nanotechnology*, Vol. 14, No. 1, 380–419, 2023.

[20] Rana, A., N. K. Sharma, S. Bera, A. Yadav, G. Gupta, and A. S. Rana, "Tuning the plasmonic resonance in TiN refractory metal," *Scientific Reports*, Vol. 14, No. 1, 7905, 2024.

[21] Kavitha, S., K. V. Sairam, and A. Singh, "Investigation of plasmonic metal conductors and dielectric substrates on nano-antenna for optical wireless communication," *Progress In Electromagnetics Research B*, Vol. 95, 1–22, 2022.

[22] Kushwaha, R. K., P. Karuppanan, and L. D. Malviya, "Design and analysis of novel microstrip patch antenna on photonic crystal in THz," *Physica B: Condensed Matter*, Vol. 545, 107–112, 2018.

[23] Zare, E., H. Baghban, M. Dolatyari, G. Rostami, and A. Rostami, "Design and simulation of nano-antenna with tunable direction of radiation," *Optik*, Vol. 125, No. 12, 2891–2894, 2014.

[24] Taya, S. A., N. Doghmosh, A. A. Alkanoo, V. Dhasarathan, N. R. Ramanujam, and I. S. Amiri, "Waveguides including negative permeability and simultaneously negative permittivity and permeability materials for sensing applications," *Optik*, Vol. 228, 166147, 2021.

[25] Krishnamurthy, R., V. Revathy, K. S. J. Wilson, S. A. Taya, and I. S. Amiri, "Phonon polariton dispersion in metal-doped nanocomposite superlattice system," *Journal of Optical Communications*, Vol. 44, No. 2, 2019.

[26] Alù, A. and N. Engheta, "Theory, modeling and features of optical nanoantennas," *IEEE Transactions on Antennas and Propagation*, Vol. 61, No. 4, 1508–1517, 2013.

[27] Ordal, M. A., L. L. Long, R. J. Bell, S. E. Bell, R. R. Bell, R. W. Alexander, and C. A. Ward, "Optical properties of the metals Al, Co, Cu, Au, Fe, Pb, Ni, Pd, Pt, Ag, Ti, and W in the infrared and far infrared," *Applied Optics*, Vol. 22, No. 7, 1099–1119, 1983.

[28] Tabata, H., "Application of terahertz wave technology in the biomedical field," *IEEE Transactions on Terahertz Science and Technology*, Vol. 5, No. 6, 1146–1153, 2015.

[29] Jha, K. R. and G. Singh, "Terahertz planar antennas for future wireless communication: A technical review," *Infrared Physics & Technology*, Vol. 60, 71–80, 2013.

[30] Maier, S. A., *Plasmonics: Fundamentals and Applications*, Springer, New York, 2007.